Original Article

Intracellular ferritin heavy chain plays the key role in artesunate-induced ferroptosis in ovarian serous carcinoma cells

Tiger Koike,[1] Motoki Takenaka,[1,*] Noriko Suzuki,[1] Yoko Ueda,[1] Minako Mori,[1] Tasuku Hirayama,[2] Hideko Nagasawa,[2] and Ken-ichirou Morishige[1]

[1]Department of Obstetrics and Gynecology, Gifu University School of Medicine, 1-1 Yanagido, Gifu 501-1194, Japan
[2]Laboratory of Pharmaceutical and Medical Chemistry, Gifu Pharmaceutical University, 1-25-4 Daigaku-Nishi, Gifu 501-1196, Japan

(Received 30 June, 2021; Accepted 24 November, 2021; Released online in J-STAGE as advance publication 25 January, 2022)

Artesunate, an antimalarial drug, induces ferroptosis, but the mechanism is still unclear. In the present study, we investigated how Artesunate induces ferroptosis in ovarian serous carcinoma. Experiments were performed using the ovarian serous carcinoma cell lines CaOV3 and SKOV3ip1, and the sensitivity of CaOV3 to Artesunate was higher than that of SKOV3ip1. Ferroptosis inhibitors inhibited Artesunate-induced intracellular lipid peroxidation and cell death. However, unlike class 1 ferroptosis inducer erastin, Artesunate had no effect on intracellular glutathione-SH levels. We found that Artesunate-induced changes in lysosomal Fe^{2+} were parallel to the induction of ferroptosis. Therefore, ferritin, which oxidizes and binds intracellular Fe^{2+}, may have an inhibitory effect on ferroptosis. Knockdown of nuclear coactivator 4, a key molecule of ferritinophagy (ferritin-specific autophagy), suppressed Artesunate-induced cell death. Knockdown of ferritin heavy chain by siRNA greatly enhanced the sensitivity to Artesunate, and overexpression of ferritin heavy chain greatly reduced the sensitivity of ovarian cancer cell lines to Artesunate. These results can explain the differential sensitivity of CaOV3 and SKOV3ip1 to Artesunate. In conclusion, enhancement of ferritinophagy is an important step involved in the mechanism of Artesunate-induced ferroptosis, and ferritin heavy chain levels may contribute to the regulation of sensitivity in Artesunate-induced ferroptosis in ovarian serous carcinoma cells.

***Key Words*:** **Artesunate, ferritinophagy, ferritin heavy chain, ferroptosis, ovarian cancer**

Ferroptosis is a novel non-apoptotic programmed cell death characterized by the requirement for both iron and lipid peroxidation that was discovered in 2012 during the search for therapeutic agents for RAS mutant cancer cells.(1) Ferritinophagy, discovered in 2014, is a ferritin-specific autophagy for intracellular iron homeostasis, and the ferritin-specific cargo receptor, nuclear coactivator 4 (NCOA4), was also identified as an essential key molecule for ferritinophagy at the same time.(2) Ferritinophagy results in an increase in intracellular Fe^{2+} and eventually enhances the Fenton reaction, generates reactive oxygen species (ROS), and promotes the induction of ferroptosis.(3) Artesunate (ART), an artemisinin compound and first-line drug in the treatment of malaria,(4) was also discovered to be a ferroptosis-inducing agent.(5) However, its detailed mechanism of action remains unclear.

Recent studies showed that ART induces ferroptosis in mutationally active KRAS pancreatic ductal adenocarcinoma cells(6) and some other cells(7,8) including ovarian cancer cell lines.(9) Furthermore, it is suggested that the possible mechanism of ART is ferritinophagy.(10)

Ferritin heavy chain (FTH), together with ferritin light chain, is one of the subunits of ferritin and is a substance that acts as a chelator of Fe^{2+} in the cell.(11) It was previously reported that overexpression of FTH in cells ameliorated oxidative stress in the cells.(12,13)

In the present study, we tried to clarify whether ferritinophagy might be involved in ART-induced ferroptosis by modulating the activity of ferritinophagy-related proteins and using a newly developed method to visualize and quantify lysosomal Fe^{2+}.(14) We also focused on the amount of FTH in the cells and whether it affects the sensitivity to ART-induced ferroptosis.

Materials and Methods

Cell culture. Ovarian serous carcinoma CaOV3(15) cells and SKOV3ip1(16) cells were cultured in Dulbecco's modified medium (Wako, Saitama, Japan) containing 10% fetal bovine serum and 1% penicillin/streptomycin (Wako) under 5% CO_2 at 37°C. These cells were provided by the Department of Obstetrics and Gynecology, Graduate School of Medicine, Osaka University, Osaka, Japan.

Induction and inhibition of ferroptosis and autophagy. We used ART (TCI, Tokyo, Japan) and erastin (ERA) (Cayman Chemical, Ann Arbor, MI) to induce ferroptosis. Deferoxamine mesylate (DFO; Sigma-Aldrich, St. Louis, MO) and ferrostatin-1 (Fer-1; Sigma-Aldrich) were used to inhibit ferroptosis. Dimethyl sulfoxide (DMSO; Wako) was used as the control, and all drugs were adjusted to a DMSO concentration of 0.5% at the time of treatment. We used chloroquine (CQ; Sigma-Aldrich) as an autophagy inhibitor that accumulates in lysosomes and increases the lysosomal pH and N2, N4-*bis*(phenylmethyl)-2,4-quinazolinediamine (DBeQ; Cayman Chemical) as a p97 ATPase inhibitor that does not inhibit the function of lysosomes but inhibits autophagy by inhibiting autophagosome maturation.

Detection of cell viability. Cell viability was tested with WST-1 reagent, Premix WST-1 Cell Proliferation Assay System (Roche, Basel, Switzerland), according to the manufacturer's instructions. Briefly, 4×10^3 cells/well were seeded in a 96-well plate and treated with different drugs at various concentrations for the indicated times. After the addition of 10 µl Premix WST-1 solution to each well, cells were incubated at 37°C for another 1 h, and the absorbance was determined at 440 nm using a microplate reader.

Detection of intracellular glutathione-SH levels. Cells were plated in 10-cm dishes at a density of 3×10^6 cells/well and

*To whom correspondence should be addressed.
E-mail: bridge@gifu-u.ac.jp

doi: 10.3164/jcbn.21-82

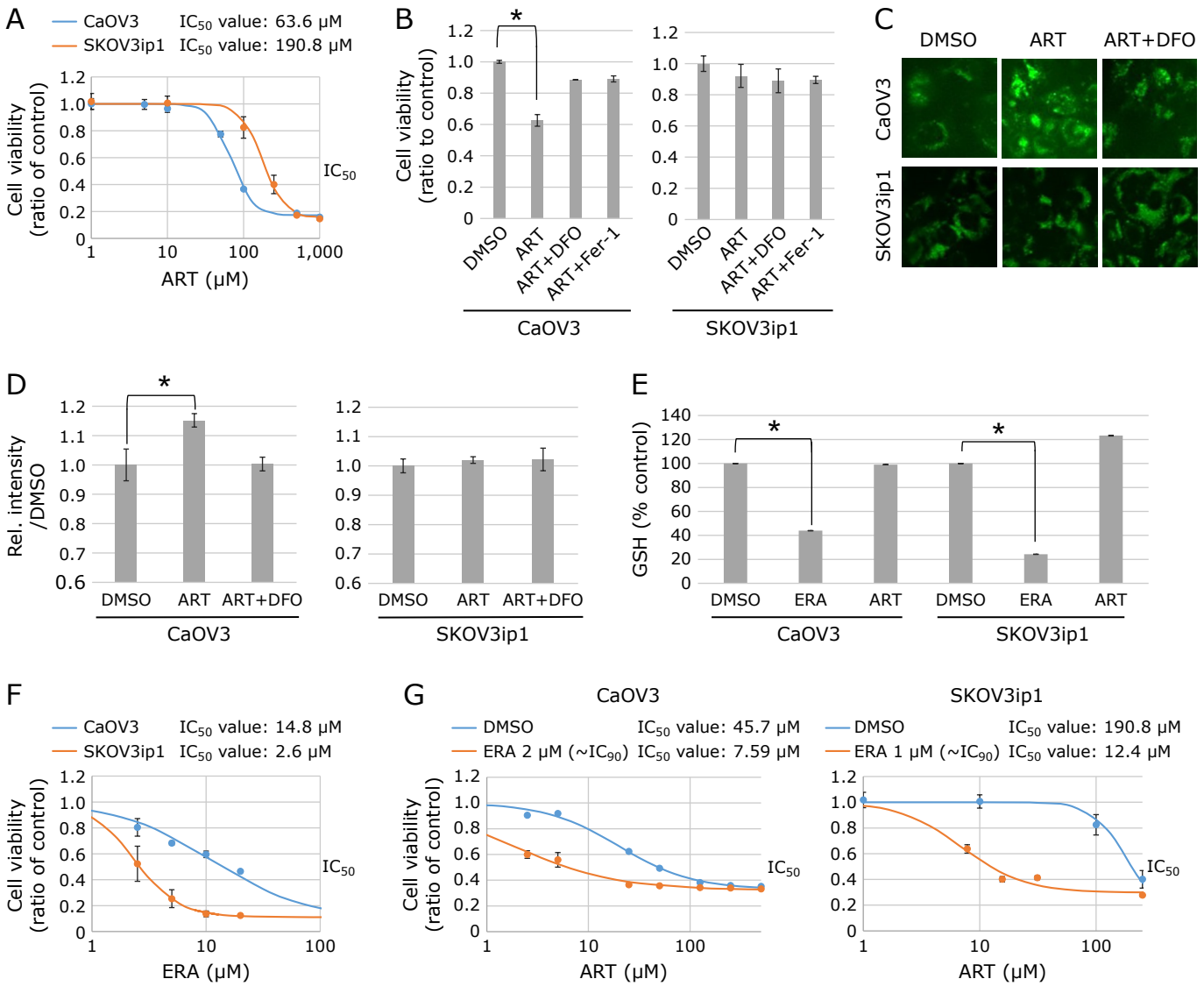

Fig. 1. Analysis of ART-induced cell death. (A) Effect of ART treatment on cell viability of CaOV3 and SKOV3ip1 cells. (B) Effect of DFO (100 μM) and Fer-1 (0.5 μM) on ART (70 μM)-induced reduction of cell viability in CaOV3 cells. (C, D) Effect of DFO (100 μM) on ART (70 μM)-enhanced lipid peroxidation in CaOV3 cells. C represents profile of BODIPY 581/591 C11. (E) Effect of ERA and ART on intracellular GSH levels in CaOV3 and SKOV3ip1 cells. (F) Effect of ERA treatment on cell viability of CaOV3 and SKOV3ip1 cells. (G) Effect of ART treatment in the presence or absence of ERA [CaOV3: 2 μM (~IC_{90}), SKOV3ip1: 1 μM (~IC_{90})] on cell viability of CaOV3 and SKOV3ip1 cells. DMSO was used as control. All cells were treated for 5 h. $n = 5$, *$p<0.05$.

cultured overnight. Cells received different treatment for 5 or 24 h followed by harvesting to determine cell number. Live cells from each sample were counted and transferred to new tubes, washed in phosphate-buffered saline (TaKaRa, Tokyo, Japan) and centrifuged twice at 1,200 rpm at 4°C for 5 min. The cell pellet was resuspended in 80 μl protein removal solution, thoroughly incorporated, cooled to −70°C and sequentially warmed to 37°C for fast freezing and thawing, kept at 4°C for 5 min, and then centrifuged at 10,000 × *g* for 10 min. The supernatant was used to determine the amount of glutathione-SH (GSH) in the sample. We used a GSSG (oxidized glutathione)/GSH quantification kit (Dojindo, Kumamoto, Japan) and followed the product instructions to determine GSH levels. This assay is based on the continued enzymatic regeneration of reduced GSH from the reduction of GSSG by the enzyme glutathione reductase and the GSH-mediated reduction of DTNB to a chromogenic product. The absorbance of GSH was read at 415 nm using a microtiter-plate ELISA reader and adjusted by cell number.

Western blotting. Protein (30 μg) was analyzed by SDS-PAGE and transferred to a polyvinylidene difluoride membrane. Proteins were detected using primary antibodies, anti-NCOA4 (ab86707, 1:500; Abcam, Cambridge, UK), anti-glutathione peroxidase 4 (GPx4) (ab125066, 1:1,000; Abcam), anti-light chain 3 beta (LC3B) (NB600-1384, 1:1,000; Novus Biologicals, CO), anti-P62 (sc-28359, 1:500; Santa Cruz Biotechnology, Santa Cruz, CA), anti-ferritin (ab75973, 1:1,000; Abcam), anti-FTH (sc-376594, 1:1,000; Santa Cruz Biotechnology), and GAPDH (FL-335, 1:500; Santa Cruz Biotechnology). Secondary antibodies were anti-mouse IgG (sc-2005, 1:2,000; Santa Cruz Biotechnology) for P62 and anti-rabbit IgG (sc-2004, 1:2,000; Santa Cruz Biotechnology) for NCOA4, GPx4, LC3B, ferritin, FTH, and GAPDH. ECL Plus blotting detection reagents (GE Healthcare, Chicago, IL) were used according to the manufacturer's instructions.

Quantification of intracellular lipid peroxidation. Lipid peroxidation in cells was tested using BODIPY 581/591 C11

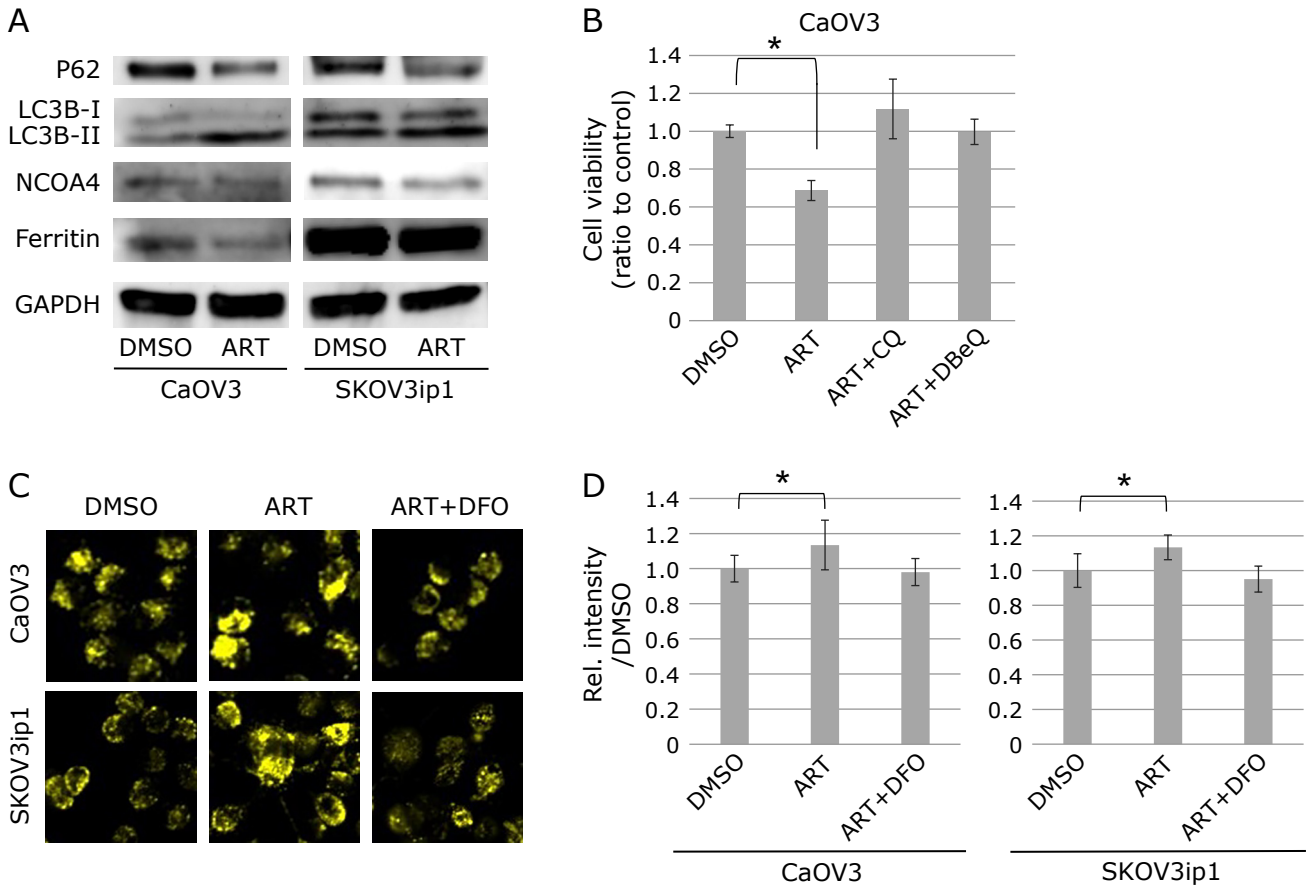

Fig. 2. Analysis of ART-induced autophagy and ferroptosis. (A) Effect of ART (70 μM) treatment for 24 h on profile of Western blot analysis in CaOV3 and SKOV3ip1 cells. (B) Effect of CQ (25 μM) and DBeQ (5 μM) on ART (70 μM)-induced reduction of cell viability in CaOV3 cells after 24 h of treatment. (C, D) Effect of DFO (100 μM) and CQ (25 μM) on ART (70 μM)-induced intracellular Fe^{2+} in CaOV3 and SKOV3ip1 cells after 5 h of treatment. C represents profile of Lyso-RhoNox. DMSO was used as control. $n = 7$, *$p<0.05$.

Lipid Peroxidation Sensor (D3861; Thermo Fisher Scientific, Waltham, MA). Cells were treated with ART (70 μM) in the presence or absence of DFO (100 μM), CQ (25 μM), and DBeQ (5 μM) for 24 h as mentioned above and stained with BODIPY 581/591 C11 in Hanks' Balanced Salt Solution (HBSS; Wako) at 37°C for 30 min. Cells were washed with HBSS and then imaged. The regions of interest were selected by setting thresholds with the default program for dark background in ImageJ.[17]

Imaging of intracellular labile Fe^{2+} level. Lysosomal labile Fe^{2+} level was estimated using the lysosomal Fe^{2+}-specific fluorescent probe (Lyso-RhoNox, Pearson's correlation value with LysoTracker® Green DND-26 = 0.80 ± 0.02) as described in our previous report.[14] RhoNox-4, another Fe^{2+}-specific fluorescent probe, was synthesized and used for evaluating subcellular labile Fe^{2+} as described in our previous report.[18] Cells were treated with ART (70 μM) in the presence or absence of DFO (100 μM) and CQ (25 μM) for 24 h as mentioned above and stained with Lyso-RhoNox or RhoNox-4 in HBSS at 37°C for 1 h. Cells were washed with HBSS and then imaged. The regions of interest were selected by setting thresholds with the default program for dark background in Image J.[17]

Gene silencing and overexpression. NCOA4 siRNA (AM16708, siRNA ID: 107705; Thermo Fisher Scientific) and FTH siRNA (sc-40575; Santa Cruz Biotechnology) were used for gene silencing. Negative Universal Control (NC) (Thermo Fisher Scientific) was used for negative control. Cells were transfected using Lipofectamine RNAiMAX (Thermo Fisher Scientific) for 72 h, and NCOA4 and FTH expressions were verified by Western blotting.

FTH1 cDNA plasmid (RC209845; OriGene, Rockville, MD) was used for gene overexpression. pCMV6-Entry Mammalian Expression Vector [empty vector (EV), PS100001; OriGene] were used for negative control. Cells were transfected using TransIT-LT1 (Mirus Bio Corporation, Madison, WI) for 72 h, and FTH expression was verified by Western blotting.

Statistical analysis. Results are presented as the mean ± SD. All data were subjected to analysis of variance, and differences between groups were assessed using Bartlett's test. Statistical analyses were performed using the ANOVA LSD test for unpaired data. A value of $p<0.05$ was assumed to indicate statistical significance. All statistical analyses were performed with EZR[19] ver. 1.52, which is for R. It is a modified version of R commander designed to add statistical functions frequently used in biostatistics.

Results

ART induces iron-dependent cell death in ovarian carcinoma cells. Cell viability of cell lines CaOV3 and SKOV3ip1 was inhibited by ART in a concentration-dependent manner (Fig. 1A), and CaOV3 was more sensitive ($p<0.05$) to ART than was SKOV3ip1. ART-induced reduction of cell viability was reversed by DFO and Fer-1 (Fig. 1B). ART enhanced intracellular lipid peroxidation and DFO cancelled this effect (Fig. 1C and D).

ERA (20 μM) drastically reduced the intracellular GSH level (Fig. 1E) after 5 h of treatment when cell viability was not

doi: 10.3164/jcbn.21-82

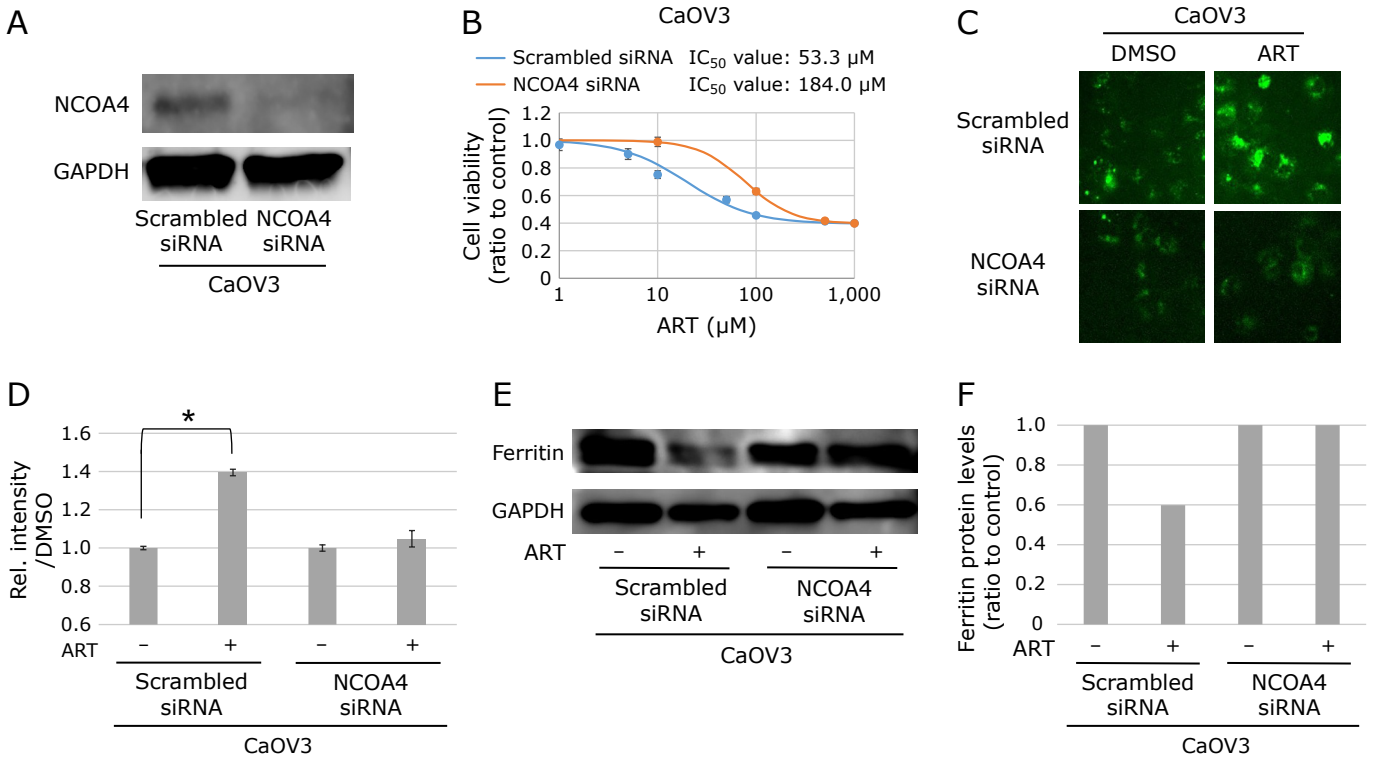

Fig. 3. Effect of knockdown of NCOA4 on ART-induced ferroptosis. (A) Profile of Western blot analysis after transfection of NCOA4 siRNA. (B) Effect of NCOA4 knockdown on ART-induced reduction of cell viability in CaOV3 and SKOV3ip1 cells. (C, D) Effect of NCOA4 knockdown on ART (70 μM)-enhanced lipid peroxidation in CaOV3 cells. C represents profile of BODIPY 581/591 C11. (E, F) Profile of Western blot analysis after transfection of NCOA4 siRNA and treated by ART in CaOV3 cells. All cells were treated for 24 h. Scrambled siRNA was used as control. Number of samples = 7, *p<0.05.

reduced (data not shown), and ERA induced ferroptosis in the CaOV3 and SKOV3ip1 cells after 24 h of treatment (data not shown). In contrast, ART showed no effect on the GSH level in CaOV3 and SKOV3ip1 cells.

Cell viability of cell lines CaOV3 and SKOV3ip1 was inhibited by ERA in a concentration-dependent manner (Fig. 1F), and SKOV3ip1 was more sensitive (p<0.05) to ERA than was CaOV3. Furthermore, we examined the additive effects of ERA to ART. CaOV3 and SKOV3ip1 cells were treated by ART in the presence or absence of ERA, and we confirmed the dose response effect of ART under rather low concentration of ERA (approximately equal to IC_{90}: 2 μM (CaOV3), 1 μM (SKOV3ip1)) (Fig. 1G). We found the synergistic effects in both CaOV3 and SKOV3ip1 cell lines.

ART-induced autophagy leads to ferroptosis in ovarian carcinoma cells. Treatment with ART decreased autophagy-related marker protein P62 and microtubule-associated protein LC3B-I and increased LC3B-II (Fig. 2A). The protein levels of NCOA4 and ferritin were also reduced after ART treatment (Fig. 2A). As shown in Fig. 2B, ART-induced ferroptosis was completely reversed by CQ or DBeQ. ART (70 μM) significantly increased Fe^{2+} in the lysosomes and co-treatment with DFO (100 μM) cancelled it (Fig. 2C and D). However, ART did not induce any change of subcellular Fe^{2+} detected by RhoNox-4 (data not shown).

Ferritinophagy is important in ART-induced ferroptosis. NCOA4 siRNA was transfected into CaOV3 cells, and the reduction of NCOA4 protein was confirmed by Western blotting (Fig. 3A). Knockdown of NCOA4 in CaOV3 cells decreased the sensitivity to ART (Fig. 3B) and diminished ART-induced intracellular lipid peroxidation (Fig. 3C and D). In addition, knockdown of NCOA4 canceled ART-induced decrease of ferritin expression (Fig. 3E and F).

FTH expression altered the sensitivity of ART-induced ferroptosis in ovarian serous carcinoma cells. As shown in Fig. 2A, the basal ferritin levels were different between the two cell lines, which might contribute to the different ART sensitivities of cell viability. We tried to confirm this possibility using transfected FTH siRNA or FTH cDNA plasmid, and scrambled siRNA and EV were used as control (Fig. 4A and G). In the transfected cells, ART reduced cell viability in a concentration-dependent manner. In SKOV3ip1 cells, FTH-silenced cells were more sensitive (p<0.05) to ART than was the control (Fig. 4B). Intracellular lipid peroxidation was also increased by ART (70 μM) in the FTH-silenced SKOV3ip1 cells (Fig. 4C and D), and ART (70 μM) significantly increased the amount of lysosomal Fe^{2+} in both cell types (Fig. 4E and F).

The CaOV3 cells with FTH overexpression were more resistant (p<0.05) to ART than was the control (Fig. 4H). Intracellular lipid peroxidation was not increased by ART (70 μM) in the CaOV3 cells with FTH overexpression (Fig. 4I and J). Further, we found that treatment with ART (70 μM) significantly increased lysosomal Fe^{2+} in both cell types (Fig. 4K and L), suggesting that ART-induced ferritinophagy actually occurs in the transfected cells.

Discussion

Serous carcinoma is the most common histological type of ovarian cancer in Japan at 33%.[20] Therefore, we used two ovarian serous carcinoma cell lines (CaOV3 and SKOV3ip1) to clarify the mechanism of ART-induced cell death.

First, ART-induced ferroptosis was compared with ERA-induced ferroptosis using two ovarian carcinoma cell lines. Treatment with ERA significantly decreased intracellular GSH levels, whereas ART did not decrease them, and this finding was consistent with that of a previous report.[21] Therefore, mechanisms of

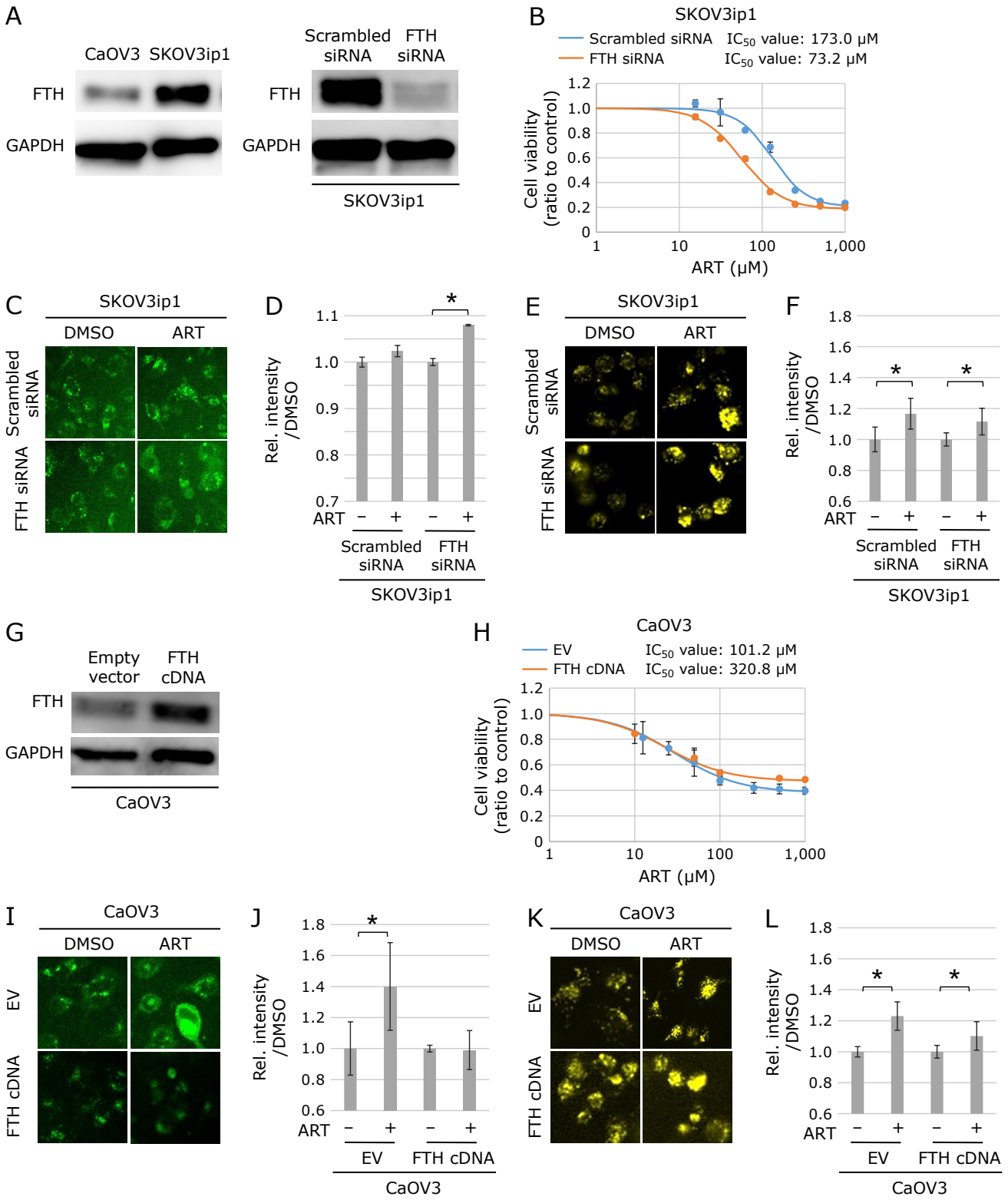

Fig. 4. Effect of FTH gene modulation on ART-induced cell death. (A) Profile of FTH level by Western blotting analysis in CaOV3 and SKOV3ip1 cells and FTH silenced in SKOV3ip1 cells by siRNA transfection. (B) Effect of FTH silencing on ART-induced reduction of cell viability in CaOV3 and SKOV3ip1 cells after 24 h of treatment. (C, D) Effect of FTH silencing on ART (70 μM)-enhanced lipid peroxidation in SKOV3ip1 cells after 24 h of treatment. C represents profile of BODIPY 581/591 C11. $n = 7$. (E, F) Effect of FTH silencing on ART (70 μM)-induced intracellular Fe^{2+} in SKOV3ip1 cells after 5 h of treatment. E represents profile of Lyso-RhoNox. $n = 7$. (G) Western blotting analysis showed that FTH was overexpressed in CaOV3 cells through cDNA plasmid transfection. (H) Effect of FTH overexpression on ART-induced reduction of cell viability in CaOV3 after 24 h of treatment. $n = 5$. (I, J) Effect of FTH overexpression on ART (70 μM)-enhanced lipid peroxidation in CaOV3 cells after 24 h of treatment. I represents profile of BODIPY 581/591 C11. $n = 7$. (K, L) Effect of FTH overexpression on ART (70 μM)-induced intracellular Fe^{2+} in CaOV3 cells after 5 h of treatment. K represents profile of Lyso-RhoNox. $n = 7$. DMSO was used as vehicle and scrambled siRNA and empty vector (EV) were used as control. FTH cDNA represents FTH overexpression. *$p<0.05$.

doi: 10.3164/jcbn.21-82

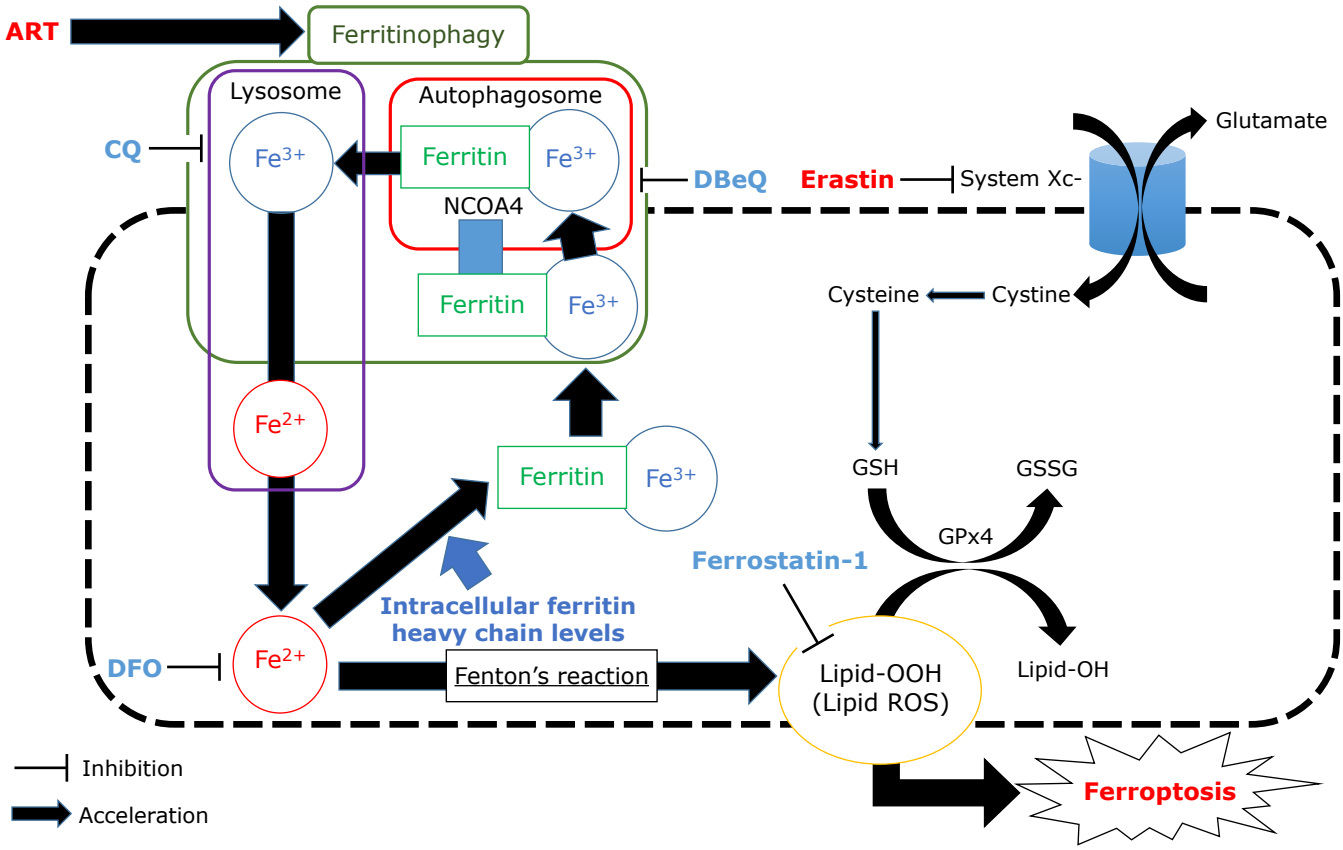

Fig. 5. Role of FTH in ART-induced ferroptosis in ovarian serous carcinoma. FTH inhibits ferroptosis by chelating intracellular Fe^{2+} and suppressing lipid peroxidation.

ferroptosis by ART and ERA were apparently different, and induction of ferroptosis by ART could take place through a pathway without affecting intracellular GSH levels. We also confirmed the combinatorial effect of ART and ERA, and we found synergistic effects in both CaOV3 and SKOV3ip1 cell lines as a previous report which confirmed the combinatorial effect of dihydroartemisinin, one of the artemisinin compounds, and ERA.[22] This result also suggests that ART and ERA induce ferroptosis by different mechanisms.

In the present study, we found that treatment with ART induced enhancement of ferritinophagy. Ferritinophagy is expected to lead to an increase in lysosomal Fe^{2+} followed by an increase in cytosolic Fe^{2+}; however, there are no reports of direct visualization of Fe^{2+} in lysosomes by ART treatment to our knowledge. Therefore, we measured the amount of Fe^{2+} in lysosomes with a new tool, Lyso-RhoNox, that we recently developed.[14] This is the first report of the direct visualization of the increase in Fe^{2+} in lysosomes.

However, for evaluation of ferritinophagy-related dynamics of cytosolic Fe^{2+}, there are no probes available at present that can specifically detect cytosolic iron in a strict sense. We used RhoNox-4, a newly developed tool to detect intracellular Fe^{2+},[18] to confirm the effect of ART and could not detect the intracellular Fe^{2+} change at 5 h after the addition of ART when the increase of lysosomal Fe^{2+} was observed. Since RhoNox-4 is not exactly specific to cytosolic Fe^{2+},[18] we speculate that the probe could not detect the change in the cytosolic Fe^{2+} induced by ART. It is also possible that Fe^{2+} released into cytosol was immediately scavenged by cytosolic iron chaperones such as Poly-(rC)-binding protein 1(PCBP1) and PCBP2,[23,24] and these rapid metabolic turnovers of cytosolic Fe^{2+} may be related to the difficulty of detecting the ART-induced change in cytosolic Fe^{2+}. This is a limitation of this study and further study is necessary to confirm change of cytosolic Fe^{2+} by ART using more specific detectors for cytosolic Fe^{2+}.

As shown in Fig. 5, the initial event of ART-induced ferroptosis may be triggered by ferritinophagy. Although the response of ART-induced cell viability was different between CaOV3 and SKOV3ip1, ferritinophagy was similarly observed in both cell types.

Interestingly, we found a difference in basal ferritin levels between the two cell lines and hypothesized that FTH may buffer ferroptosis through a mechanism by which cytoplasmic Fe^{2+} is converted to Fe^{3+} and binds to ferritin. FTH catalyzes the conversion of Fe^{2+} to Fe^{3+} and increases the intracellular storage of inactive Fe^{3+},[11] and overexpression of FTH in HeLa cells and glioma cells has been reported and resulted in the amelioration of oxidative stress in cells.[12,13] Mumbauer *et al.*[25] also reported the role of FTH in ferroptosis. When FTH was knocked down during wing development in *Drosophila melanogaster*, significant defects were observed in adult wing growth by enhanced ferroptosis.[25] These reports support our finding that high FTH levels in SKOV3ip1 cells showed stronger resistance to ART-induced ferroptosis than that in CaOV3 cells, and the amount of FTH may affect the susceptibility to ART-induced ferroptosis.

In addition, we found that ART-induced ferroptosis was increased in FTH-silenced cells and decreased in cells that overexpressed it. However, ART treatment significantly increased lysosomal Fe^{2+} levels in both FTH-silenced and FTH-overexpressing cells, suggesting that FTH levels do not modulate lysosomal Fe^{2+} levels. In contrast, treatment with ART increased intracellular lipid peroxidation in FTH-silenced cells of ferroptosis-resistant SKOV3ip1, suggesting that FTH silencing conferred susceptibility to ferroptosis, and ART did not cause

intracellular lipid peroxidation in FTH-overexpressing CaOV3 cells, suggesting that FTH overexpression acquired ferroptosis resistance. Taking these findings together, we speculate that the pathway to ART-induced ferroptosis may be inhibited by a very high basal level of FTH and reduced release of Fe^{2+} from ferritin-bound iron, which is characteristic of cells such as SKOV3ip1 cells, in which the ferritin complex is fully capable of storing iron as Fe^{3+}. ART induces ferritinophagy in both cell types, but ferroptosis may be induced in cells with low basal levels of ferritin, as shown in Fig. 5.

This is the first report showing that the intracellular FTH level in ovarian serous carcinoma cells is one of the important factors determining their susceptibility to ART-induced ferroptosis and that silencing of the FTH gene is effective in improving resistance to ART-induced ferroptosis. Because we did not confirm the results *in vivo* in this study, further studies will be needed.

Author Contributions

Conception, design and development of methodology: TK, MT, NS, TH, HN, and KM. Data gathering, analysis and interpretation: TK, MT, NS, YU, MM, TH, and HN. Writing, review and/or revision of the paper: TK, MT, NS, YU, MM, TH, HN, and KM. All authors read and approved the final paper.

Acknowledgments

This work was supported by MEXT KAKENHI Grant Number 18K09257 and a Grant for Clinical Research Promotion from Gifu University and Gifu Pharmaceutical University.

The authors thank the Department of Obstetrics and Gynecology, Graduate School of Medicine, Osaka University, Osaka, Japan for providing the CaOV3 and SKOV3ip1 cells.

Abbreviations

ART	artesunate
CQ	chloroquine
DBeQ	N2, N4-*bis*(phenylmethyl)-2,4-quinazolinediamine
DFO	deferoxamine mesylate
DMSO	dimethyl sulfoxide
ERA	erastin
EV	empty vector
Fer-1	ferrostatin-1
FTH	ferritin heavy chain
GPx4	glutathione peroxidase 4
GSH	glutathione-SH
HBSS	Hanks' Balanced Salt Solution
LC3B	light chain 3 beta
NCOA4	nuclear coactivator 4
ROS	reactive oxygen species

Conflict of Interest

No potential conflicts of interest were disclosed.

References

1 Dixon SJ, Lemberg KM, Lamprecht MR, *et al*. Ferroptosis: an iron-dependent form of nonapoptotic cell death. *Cell* 2012; **149**: 1060–1072.
2 Mancias JD, Wang X, Gygi SP, Harper JW, Kimmelman AC. Quantitative proteomics identifies NCOA4 as the cargo receptor mediating ferritinophagy. *Nature* 2014; **509**: 105–109.
3 Masaldan S, Clatworthy SAS, Gamell C, *et al*. Iron accumulation in senescent cells is coupled with impaired ferritinophagy and inhibition of ferroptosis. *Redox Biol* 2018; **14**: 100–115.
4 Dondorp A, Nosten F, Stepniewska K, Day N, White N; South East Asian Quinine Artesunate Malaria Trial (SEAQUAMAT) group. Artesunate versus quinine for treatment of severe falciparum malaria: a randomised trial. *Lancet* 2005; **366**: 717–725.
5 Ooko E, Saeed ME, Kadioglu O, *et al*. Artemisinin derivatives induce iron-dependent cell death (ferroptosis) in tumor cells. *Phytomedicine* 2015; **22**: 1045–1054.
6 Eling N, Reuter L, Hazin J, Hamacher-Brady A, Brady NR. Identification of artesunate as a specific activator of ferroptosis in pancreatic cancer cells. *Oncoscience* 2015; **2**: 517–532.
7 Roh JL, Kim EH, Jang H, Shin D. Nrf2 inhibition reverses the resistance of cisplatin-resistant head and neck cancer cells to artesunate-induced ferroptosis. *Redox Biol* 2017; **11**: 254–262.
8 Wang N, Zeng GZ, Yin JL, Bian ZX. Artesunate activates the ATF4-CHOP-CHAC1 pathway and affects ferroptosis in Burkitt's Lymphoma. *Biochem Biophys Res Commun* 2019; **519**: 533–539.
9 Greenshields AL, Shepherd TG, Hoskin DW. Contribution of reactive oxygen species to ovarian cancer cell growth arrest and killing by the anti-malarial drug artesunate. *Mol Carcinog* 2017; **56**: 75–93.
10 Kong Z, Liu R, Cheng Y. Artesunate alleviates liver fibrosis by regulating ferroptosis signaling pathway. *Biomed Pharmacother* 2019; **109**: 2043–2053.
11 Harrison PM, Arosio P. The ferritins: molecular properties, iron storage function and cellular regulation. *Biochim Biophys Acta* 1996; **1275**: 161–203.
12 Cozzi A, Corsi B, Levi S, Santambrogio P, Albertini A, Arosio P. Overexpression of wild type and mutated human ferritin H-chain in HeLa cells: *in vivo* role of ferritin ferroxidase activity. *J Biol Chem* 2000; **275**: 25122–25129.
13 Chen Y, Li N, Wang H, *et al*. Amentoflavone suppresses cell proliferation and induces cell death through triggering autophagy-dependent ferroptosis in human glioma. *Life Sci* 2020; **247**: 117425.
14 Hirayama T, Miki A, Nagasawa H. Organelle-specific analysis of labile Fe(ii) during ferroptosis by using a cocktail of various colour organelle-targeted fluorescent probes. *Metallomics* 2019; **11**: 111–117.
15 Buick RN, Pullano R, Trent JM. Comparative properties of five human ovarian adenocarcinoma cell lines. *Cancer Res* 1985; **45**: 3668–3676.
16 Yu D, Wolf JK, Scanlon M, Price JE, Hung MC. Enhanced c-erbB-2/neu expression in human ovarian cancer cells correlates with more severe malignancy that can be suppressed by E1A. *Cancer Res* 1993; **53**: 891–898.
17 Schneider CA, Rasband WS, Eliceiri KW. NIH Image to ImageJ: 25 years of image analysis. *Nat Methods* 2012; **9**: 671–675.
18 Hirayama T, Niwa M, Hirosawa S, Nagasawa H. High-throughput screening for the discovery of Iron homeostasis modulators using an extremely sensitive fluorescent probe. *ACS Sens* 2020; **5**: 2950–2958.
19 Kanda Y. Investigation of the freely available easy-to-use software 'EZR' for medical statistics. *Bone Marrow Transplant* 2013; **48**: 452–458.
20 Enomoto T. The treatment annual report in 2011. *Acta Obstet Gynaecol Jpn* 2018; **70**: 1372–1444.
21 Chen GQ, Benthani FA, Wu J, Liang D, Bian ZX, Jiang X. Artemisinin compounds sensitize cancer cells to ferroptosis by regulating iron homeostasis. *Cell Death Differ* 2020; **27**: 242–254.
22 Du J, Wang T, Li Y, *et al*. DHA inhibits proliferation and induces ferroptosis of leukemia cells through autophagy dependent degradation of ferritin. *Free Radic Biol Med* 2019; **131**: 356–369.
23 Philpott CC, Patel SJ, Protchenko O. Management versus miscues in the cytosolic labile iron pool: the varied functions of iron chaperones. *Biochim Biophys Acta Mol Cell Res* 2020; **1867**: 118830.
24 Hider RC, Kong X. Iron speciation in the cytosol: an overview. *Dalton Trans* 2013; **42**: 3220–3229.
25 Mumbauer S, Pascual J, Kolotuev I, Hamaratoglu F. Ferritin heavy chain protects the developing wing from reactive oxygen species and ferroptosis. *PLoS Genet* 2019; **15**: e1008396.

doi: 10.3164/jcbn.21-82